THE ASTROPHYSICAL JOURNAL, 482:L33–L36, 1997 June 10
© 1997. The American Astronomical Society. All rights reserved. Printed in U.S.A.

HYDRODYNAMICAL MODELS OF SUPERLUMINAL SOURCES

J. L. GÓMEZ,[1] J. M. MARTÍ,[2] A. P. MARSCHER,[3] J. M. IBÁÑEZ,[2] AND A. ALBERDI[1]
Received 1997 January 9; accepted 1997 March 21

ABSTRACT

We present numerical simulations of the generation, evolution, and radio emission of superluminal components in relativistic jets. We perform the fluid dynamical calculations using a relativistic time-dependent code based on a high-resolution shock-capturing scheme, and then we calculate the radio emission by integrating the transfer equations for synchrotron radiation. These simulations show that a temporary increase in the flow velocity at the base of the jet produces a moving perturbation that contains both a forward and a reverse shock and is trailed by a rarefaction. The perturbation appears in the simulated maps as a region of enhanced emission moving downstream at a superluminal apparent velocity. Interactions of the perturbation with the underlying steady jet result in changes in the internal brightness distribution of the superluminal component, which are manifested as low-level fluctuations about the long-term evolution of both the apparent velocity and the exponential decay of the light curves.

Subject headings: galaxies: jets — hydrodynamics — radiation mechanisms: nonthermal — relativity

1. INTRODUCTION

The ejection of radiating plasma at apparent superluminal speeds is commonly observed in the radio jets of many blazars (e.g., Pearson et al. 1981) and was recently discovered in the Galactic sources GRS 1915+105 (Mirabel & Rodríguez 1994) and GRO J1655−40 (Tingay et al. 1995; Hjellming & Rupen 1995), in what seems to be a reduced version of the same phenomenon (Sams, Eckart, & Sunyaev 1996). Apparent transverse motions at speeds greater than c can be explained by relativistic fluid motions in jets viewed at small angles to the line of sight (Blandford & Königl 1979). These ejections are usually preceded by outbursts in emission at radio wavelengths, whose frequency-dependent light curves of both total and polarized flux are successfully interpreted in terms of traveling shock waves, based on simplified hydrodynamical models (Marscher & Gear 1985; Hughes, Aller, & Aller 1991; Gómez et al. 1994). However, in order to obtain a detailed description of the generation, structure, evolution, and influence on the radio emission of these shocks, a more realistic formulation of the fluid dynamics is needed. This has become possible only recently, thanks to the development of time-dependent hydrodynamical relativistic codes (van Putten 1993, 1996; Duncan & Hughes 1994; Martí, Müller, & Ibáñez 1994; Koide, Nishikawa, & Mutel 1996). Preliminary results regarding the emission from compact radio jets using such hydrodynamical models (Gómez et al. 1995, 1996a, 1996b; Duncan, Hughes, & Opperman 1996; Komissarov & Falle 1996) have shown the power of this tool in understanding the physics of compact jets and their environments. Whereas in Gómez et al. (1995) we concentrated on the emission properties from *steady* relativistic jets, focusing on the role played by the external medium in determining the jet opening angle and presence of standing shocks, in this Letter we use a similar numerical procedure to study the ejection, structure, and evolution of superluminal components through variations in the ejection velocity at the jet inlet.

[1] Instituto de Astrofísica de Andalucía, CSIC, Apdo. 3004, Granada 18080, Spain; jlgomez@iaa.es, alberdi@laeff.esa.es.

[2] Departamento de Astronomía y Astrofísica, Universidad de Valencia, Burjassot 46100, Spain; jose-maria.marti@uv.es, jose.m.ibanez@uv.es..

[3] Department of Astronomy, Boston University, 725 Commonwealth Avenue, Boston, MA 02215; marscher@bu.edu.

2. HYDRODYNAMICAL MODELS OF SUPERLUMINAL RADIO SOURCES

Our study relies on two relativistic, axially symmetric jet models (pressure-matched, or "PM," and overpressured, or "OP"; see below) obtained by means of a high-resolution shock capturing scheme to solve the equations of relativistic hydrodynamics in cylindrical coordinates. The code is the same as that used to study large-scale relativistic jets by Martí et al. (1995, 1997), where the differential equations, as well as their finite-difference form, and a description of exhaustive testing of the hydrodynamical code can be found. In our model, the jet material is represented by an ideal gas of adiabatic exponent 4/3. The quiescent state of both the PM and OP models corresponds to a diffuse ($\rho_b/\rho_a = 10^{-3}$), relativistic ($\Gamma_b = 4$), cylindrical beam with (local) Mach number $M_b = 1.69$. (Here ρ stands for proper rest-mass density and Γ for Lorentz factor; subscripts a and b refer, respectively, to atmosphere and beam; values correspond to the injection position). Model PM has $p_b = p_a$ (pressure matched at injection position), while model OP has $p_b = 1.5p_a$ (overpressured). Pressure in the atmosphere follows the law $p(z) = p_a/[1 + (z/z_c)^n]^{(m/n)}$, where $z_c = 60R_b$ (R_b is the beam cross-sectional radius at injection position) represents the pressure "scale height" in the axial direction, $n = 1.5$, and $m = 2.3$. We do not intend to model the expected complex atmosphere, but only to produce a pressure gradient large enough to induce the observed opening angles in compact jets by fixing z_c, n, and m at suitable values.

To obtain the steady jet, we start with a jet of constant radius, velocity, density, and internal energy extending across the whole grid. The decreasing atmosphere causes the beam to become overpressured outside the injection point and pressure equilibrium is established through radial expansion of the jet. During the time needed for the jet to reach the stationary state (typically 2–5 longitudinal grid light-crossing times) the external pressure gradient should remain steady. This has been obtained by adding an external force that maintains the pressure gradient, without disturbing significantly the jet dynamics (see below). Other possibilities to keep the ambient pressure gradient constant outside the jet were rejected given the inherent difficulties found in the precise determination of

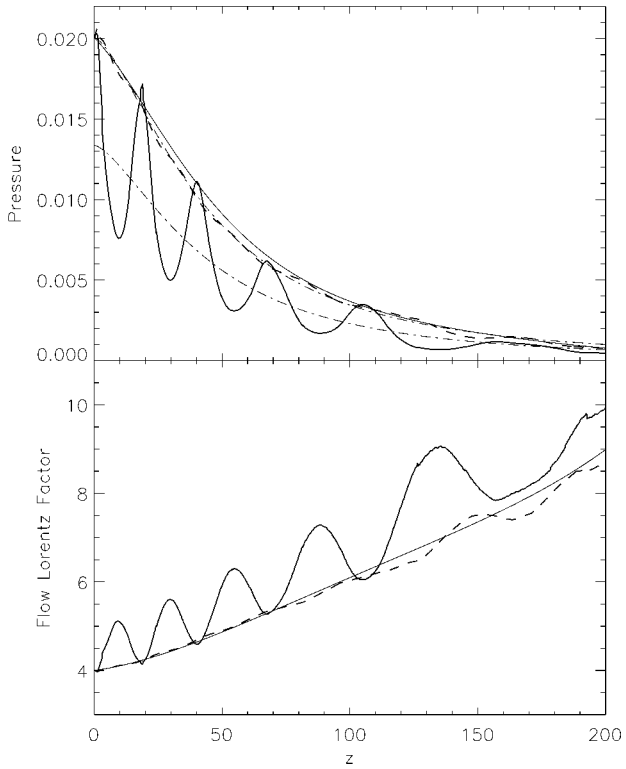

FIG. 1.—(*a*) Pressure distribution and (*b*) flow Lorentz factor, averaged over the cross section, along the jet for models PM (*thick dashed lines*) and OP (*thick solid lines*). Thin solid line corresponds to adiabatic evolution of a jet with local opening angle as for model PM. Dot-dashed lines in (*a*) correspond to the pressure distribution in the external medium for models PM (*upper line*) and OP (*lower line*).

the beam/atmosphere boundary (which is affected by numerical diffusion).

2.1. *PM Versus OP Steady Jet Models*

Values of pressure and flow Lorentz factor (averaged over the cross section of the jet) along the jet are plotted in Figure 1 for both PM and OP steady jet models. Plotted models correspond to time $t = 900R_b/c$, just before the introduction of the perturbation. At this time, stationarity is complete along the first 100 R_b (with variations smaller than 1%) whereas some degree of variation (<10%) is still observed in the second half of the grid. Figure 1 shows that the external pressure gradient is gentle enough to allow the originally pressure matched jet (model PM) to reach equilibrium with the atmosphere smoothly (see Fig. 1*a*). On the contrary, the initial pressure mismatch in model OP is responsible for the series of oblique shocks and rarefactions seen as variations in Figures 1*a*–1*b* (see also the steady state models in Fig. 2 below). The strength and spacing of these internal shocks are determined by the Mach number and the gradient in the external pressure (Daly & Marscher 1988; Bowman 1994; Gómez et al. 1995).

Comparison of numerical models PM and OP with an adiabatically expanding (in the absence of external forces) jet calculation (thicker solid lines in Figs. 1*a*–1*b*) shows that model PM fits quite well with the expected adiabatic behavior and proves that the extra force added to balance the external pressure gradient does not affect the jet dynamics. In fact, the relativistic Bernoulli law is fulfilled along the stationary beam to within 5% accuracy. Model OP, on the contrary, reaches the PM jet values at compressions, showing large variations of pressure, rest-mass density, internal energy, and flow Lorentz factor between maxima and minima.

2.2. *Generation and Evolution of Traveling Perturbations*

In this *Letter* we concentrate our attention on the study of the evolution of the flow after a square-wave increase of the beam flow velocity in both PM and OP models, from the quiescent value $\Gamma_b = 4$, to $\Gamma_p = 10$ during a short period of time $\tau_p = 0.75$. Because of the faster flow velocity in the perturbation, the fluid in front piles up, creating a shocked state (S) in which the pressure and the rest-mass density are higher than in the quiescent state. The leading shock propagates at $\Gamma_{SH} = 10$. A rarefied state (R) develops behind the perturbation. The pressure mismatch between these components (S, R) and the external medium causes the transverse section of the beam to change with respect to the steady model. The shocked region expands laterally into the external medium, which has a pressure p_a smaller than p_S. In the rarefied region, on the contrary, since $p_R < p_a$, the beam reduces its radius.

Results with the dynamical evolution of the perturbation in both models PM and OP are shown in Figure 2 (Plate L2), which contains two sets of panels showing the pressure distribution at different epochs. The first panel of each corresponds to the quiescent jet. [The flow is better represented as a movie than as the "snapshots" presented here; the reader is referred to the lead author's World Wide Web site at http://www.iaa.es/~jlgomez/jets.html at which the (hydrodynamic and emission) movies can be viewed.] Both the shocked and rarefied regions in the perturbation are clearly seen. When the perturbation passes through a standing shock, the latter is "dragged" downstream for some distance before returning to its initial position as the steady jet becomes reestablished. The interaction with a rarefaction is similar, with the additional feature that a reverse shock is formed, propagating relatively slowly down the jet, before coming to a stop and dissipating (see also Gómez et al. 1996a, 1996b). The variation in beam radius due to the passage of the component is also evident. This perturbation occurring on the beam surface saturates in small oblique shocks within the beam and is responsible for small variations trailing the main perturbation near the beam axis. Although this is a minor effect, the passage of a more powerful component could excite beam radial modes at amplitudes high enough to produce strong internal shocks.

The resolution used in our calculations is not sufficient to calculate accurately the pattern speed of the component, although the results we have obtained are compatible with a component moving with Lorentz factor equal to 10 and accelerating slightly with time. Moreover, there are also indications of quasi-periodic variations of the pattern speed in model OP, associated with the passage of the perturbation through faster (more rarefied) and slower (more compressed) regions of the previously undisturbed flow. These variations in the pattern Lorentz factor may provide an alternative to geometric effects in the interpretation of the variations in the apparent motion found in many jets (e.g., 3C 345, 0836+71, 3C 454.3, 3C 273 [Zensus, Krichbaum, & Lobanov 1995, and references therein]; 4C 39.25 [Alberdi et al. 1993]; and 3C 263 [Hough, Zensus, & Porcas 1996]).

Within the resolution of our simulations, in both the PM

and OP cases the evolution of the perturbation seems to proceed without noticeable variations in the number of particles contained within it and maintains approximate self-similarity. It is also consistent with an adiabatic evolution, in concordance with the assumption of previous works (Marscher & Gear 1985; Hughes, Aller, & Aller 1989; Gómez et al. 1994).

3. RADIO EMISSION

In order to compute the radio emission from the hydrodynamical results presented above, we distribute the internal energy among the electrons following a power law and assume that the magnetic energy remains a fixed fraction of the particle energy density. The emission is then calculated by integrating the synchrotron transfer equations while accounting for relativistic effects such as Doppler boosting and light aberration (see Gómez et al. 1995, and references therein for a complete description of the emission code). Due to the highly relativistic speeds present in the jet, light-travel time delays play the most important role in the emission time evolution, especially for small viewing angles (e.g., Gómez et al. 1994, 1996a, 1996b). To account for this, the absorption and emission coefficients are calculated using a retarded time that accounts for the delays within the jet. Therefore, information on the parameters that determine the emission is needed for every cell and time step (i.e., cell size over light speed). Although this represents a significant computational effort, it allows the calculation of different emission models (i.e., different viewing angles, observation time, and frequency, etc.) with a single hydrodynamical run.

Figure 3 (Plate L3) shows the total intensity maps of optically thin synchrotron radiation corresponding to the stationary model, and four epochs in the evolution of the disturbance for the jet models PM and OP, with the jets observed at a viewing angle $\theta = 10°$. Superimposed are contours showing the emission convolved with a circular Gaussian beam as would occur in actual VLBI observations. By looking at the unconvolved stationary maps of model OP, we observe a regular pattern of knots of high emission, associated with the increased specific internal energy and rest-mass density of internal oblique shocks produced by the initial overpressure in this model. The intensity of the knots decreases along the jet due to the expansion resulting from the gradient in external pressure. VLBI cores can be interpreted as the first of the recollimation shocks in the steady jet (Daly & Marscher 1988; Gómez et al. 1995). As is illustrated by the convolved maps, the observation of these stationary structures would require very high linear resolution, now achievable through millimeter-wave and space VLBI observations. The first indications of these stationary components have been found in the radio jet of M87 (Junor & Biretta 1995)—as expected due to its relative proximity—and the superluminal galactic source GRO J1655−40 (Tingay et al. 1995). Stationary components have been found in several superluminal sources (e.g., 4C 39.25 [Alberdi et al. 1993], 0836+710 [Krichbaum et al. 1990], 0735+178 [Gabuzda et al. 1994], 3C 279 [Wehrle et al. 1997], 3C 395 [Lara et al. 1994]), which may be associated not only with periodic recollimation shocks, but also with bends in the jet (Gómez, Alberdi, & Marcaide 1993), or sudden variations in the external pressure that result in strong, isolated recollimation shocks.

In the convolved maps in Figure 3, we recognize, for both PM and OP models, the usual core-jet VLBI structure of a blazar, with a single well-defined, superluminally moving component associated with the moving shock. Note that because the maps are shown for an optically thin frequency of observation, the core reflects the ad hoc jet inlet. For model OP the core position depends on the beam size and location of the first stationary hotspot. For optically thick frequencies the core in both models reflects the observed inverted spectrum, with a frequency dependence of position of approximately $r_{\rm core} \propto \nu^{-0.8}$ (see also Gómez et al. 1993, 1995). The unconvolved maps show a much more complex jet structure. Due to the time delays, the shocked region appears as a very extended region of higher emission (Gómez et al. 1994), which is moving and interacting with the quiescent jet. As a result of this interaction, the previously stationary hotspots in model OP increase in flux, being later dragged temporarily downstream. Dragging in component K1 of 0735+178 has been observed (Gabuzda et al. 1994), and new VLBI observations of this source and the radio galaxy 3C 120 are underway to compare this behavior more closely with our model. Similar results of the interaction of superluminal and stationary components have also been observed in 3C 279 (Wehrle et al. 1997), and may be expected in other sources as more high-frequency images become available.

For model PM, the gentle decay in intensity along the jet in the stationary model might be expected to dominate the evolution of the shocked component, resulting in smoothly decreasing emission as the component propagates down the jet. However, the shocked material expands owing to its

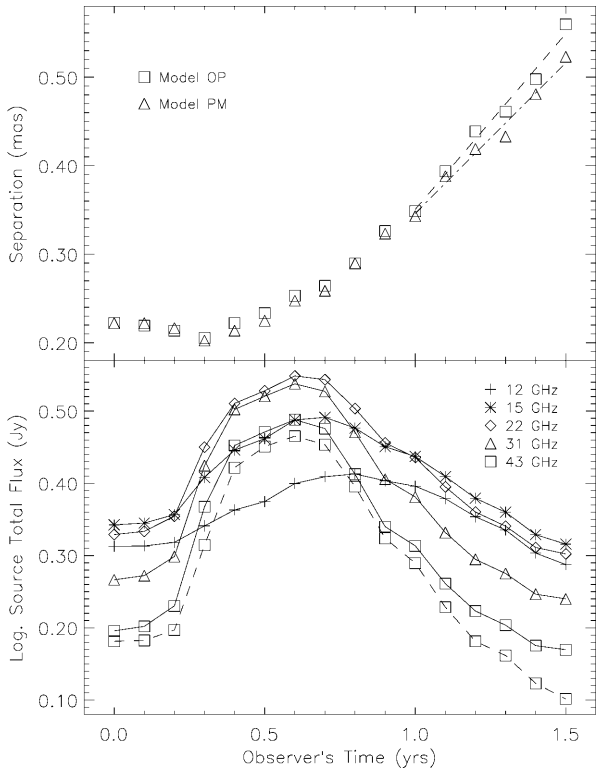

FIG. 4.—(*a*) Separation of the component observed in the convolved maps of Fig. 3 vs. time for models PM and OP. Fitting epochs 1.0 to 1.5 yr to a straight line gives apparent velocities 7.4*c* and 8.6*c* for models PM (*dot-dashed line*) and OP (*dashed line*), respectively. (*b*) Simulated multifrequency light curves for model OP, and 43 GHz light curve for model PM (with the logarithm of the flux displaced downward by 0.25 to separate it from the OP curves; the data for the PM curve are connected with a dashed line).

overpressure relative to the external medium, leading to overexpansions and overcontractions caused by inertial overshooting past equilibrium. Time delays propagate these fluctuations over the entire length of the shocked region as seen by the observer, resulting in a knotty structure in the brightness distribution of the component. The component also changes with time as the shock propagates down the jet, until the shock finally dissipates and the jet recovers its initial steady, smoothly decreasing (with distance from the input point) emission structure.

Figure 4*a* shows the separation of the brightness centroid of the moving component as a function of time for models PM (*triangles*) and OP (*squares*). Fitting the separation of the brightness centroid versus time to a straight line starting at epoch 1.0 yr, when the new component first becomes distinguishable from the core in the maps, we obtain an apparent velocity of $\sim 7.4c$ (PM model) and $\sim 8.6c$ (OP model), in general concordance with the expected value for a pattern Lorentz factor of $\Gamma \sim 10$ and viewing angle of 10°. The differences between the apparent motion of models PM and OP is due to changes in the complex underlying internal brightness distribution of the convolved components, as seen in the unconvolved maps of Figure 3.

Light curves covering the evolution of model OP are shown in Figure 4*b* for five different frequencies. The ejection of the component is accompanied by a burst in flux at all frequencies. The subsequent evolution is determined by the opacity at each frequency, reaching flux maximum when the component becomes optically thin. For frequencies at which the source becomes optically thick at a given time, this results in a slower initial increase of the flux at lower frequencies, with the flux peak higher and occurring earlier at higher frequencies. Once the maximum flux is reached the light curves show an exponential decay, in agreement with the light curves of superluminal components observed in 3C 345 (Lobanov & Zensus 1997) and the radio flares in the accreting binary system GRS 1915+105 (Foster et al. 1996). Model PM shows very similar light curves, shifted to higher fluxes and turnover frequencies, as expected by the higher mean pressure value (see Fig. 1), as shown by the dashed line in Figure 4*b*, which represents the 43 GHz light curve for model PM. Small fluctuations are apparent in the light curves of both models PM and OP, apparent at epochs 1.0 and 1.3 yr. These correspond to changes in the brightness distribution of the component, when the peak of flux moves to the subsequent knot as the component evolves along the jet (see also Fig. 3).

With further exploration of the hydrodynamics of relativistic jets, we expect to be able to explain many of the previously puzzling details in the variations of brightness, polarization, and appearance of compact radio sources.

This research is supported in part by the Spanish DGICYT (PB94-1275, PB94-0973) and by NATO grant SA.5-2-05(CRG.961228). J. L. Gómez and J. M. Martí gratefully acknowledge return grants from the Spanish Ministry of Education.

REFERENCES

Alberdi, A., Marcaide, J. M., Marscher, A. P., Zhang, Y. F., Elosegui, P., Gómez, J. L., & Shaffer, D. B. 1993, ApJ, 402, 160
Blandford, R. D., & Königl, A. 1979, ApJ, 232, 34
Bowman, M. 1994, MNRAS, 269, 137
Daly, R. A., & Marscher, A. P. 1988, ApJ, 334, 539
Duncan, G. C., & Hughes, P. A. 1994, ApJ, 436, L119
Duncan, G. C., Hughes, P. A., & Opperman, J. 1996, in ASP Conf. 100, Energy Transport in Radio Galaxies and Quasars, ed. P. E. Hardee, A. H. Bridle, & J. A. Zensus (San Francisco: ASP), 143
Foster, R. S., Waltman, E. B., Tavani, B., Harmon, B. A., Zhang, S. N., Paciesas, W. S., & Ghigo, F. D. 1996, ApJ, 467, L81
Gabuzda, D. C., Wardle, J. F. C., Roberts, D. H., Aller, M. F., & Aller, M. H. 1994, ApJ, 435, 128
Gómez, J. L., Alberdi, A., & Marcaide, J. M. 1993, A&A, 274, 55
Gómez, J. L., Alberdi, A., & Marcaide, J. M., Marscher, A. P., & Travis, J. P. 1994, A&A, 292, 33
Gómez, J. L., Martí, J. M., Marscher, A. P., Ibáñez, J. M., & Marcaide, J. M. 1995, ApJ, 449, L19
———. 1996a, in ASP Conf. 100, Energy Transport in Radio Galaxies and Quasars, ed. P. E. Hardee, A. H. Bridle, J. A. Zensus (San Francisco: ASP), 159
Gómez, J. L., Martí, J. M., Marscher, A. P., & Ibáñez, J. M. 1996b, in ASP Conf. 110, Blazar Continuum Variability, ed. H. R. Miller, J. R. Webb & J. C. Noble (San Francisco: ASP), 242
Hjellming, R. M., & Rupen, M. P. 1995, Nature, 375, 464
Hough, D. H., Zensus, J. A., & Porcas, R. W. 1996, ApJ, 464, 715
Hughes, P. A., Aller, H. D., & Aller, M. F. 1989, ApJ, 341, 54
———. 1991, ApJ, 374, 57
Junor, W., & Biretta, J. A. 1995, AJ, 109, 500
Koide, S., Nishikawa, K.-I., & Mutel, R. L. 1996, ApJ, 463, L71
Komissarov, S. S., & Falle, S. A. E. G. 1996, in ASP Conf. 100, Energy Transport in Radio Galaxies and Quasars, ed. P. E. Hardee, A. H. Bridle, & J. A. Zensus (San Francisco: ASP), 173
Krichbaum, T. P., Hummel, C. A., Quirrenbach, A., Schalinski, C. A., & Witzel, A. 1990, A&A, 230, 271
Lara, L., Alberdi, A., Marcaide, J. M., & Muxlow, T. W. B. 1994, A&A, 285, 393
Lobanov, A. P., & Zensus, J. A. 1997, ApJ, submitted
Marscher, A. P., & Gear, W. K. 1985, ApJ, 298, 114
Martí, J. M., Müller, E., Font, J. A., & Ibáñez, J. M. 1995, ApJ, 448, L105
Martí, J. M., Müller, E., Font, J. A., Ibáñez, J. M., & Marquina, A. 1997, ApJ, 479, 151
Martí, J. M., Müller, E., & Ibáñez, J. M. 1994, A&A, 281, L9
Mirabel, I. F., & Rodríguez, L. F. 1994, Nature, 371, 46
Pearson, T. J., Unwin, S. C., Cohen, M. H., Linfield, R. P., Readhead, A. C. S., Seielstad, G. A., Simon, R. S., & Walker, R. C. 1981, Nature, 290, 365
Sams, B. J., Eckart, A., & Sunyaev, R. 1996, Nature, 382, 47
Tingay, S. J., et al. 1995, Nature, 374, 141
van Putten, M. H. P. M. 1993, ApJ, 408, L21
———. 1996, ApJ, 467, L57
Wehrle, A. E., et al. 1997, in ASP Conf. 110, Blazar Continuum Variability, ed. H. R. Miller, J. R. Webb, & J. C. Noble (San Francisco: ASP), 430
Zensus, J. A., Krichbaum, T. P., & Lobanov, A. P. 1995, Proc. Nat. Acad. Sci., 92, 11348

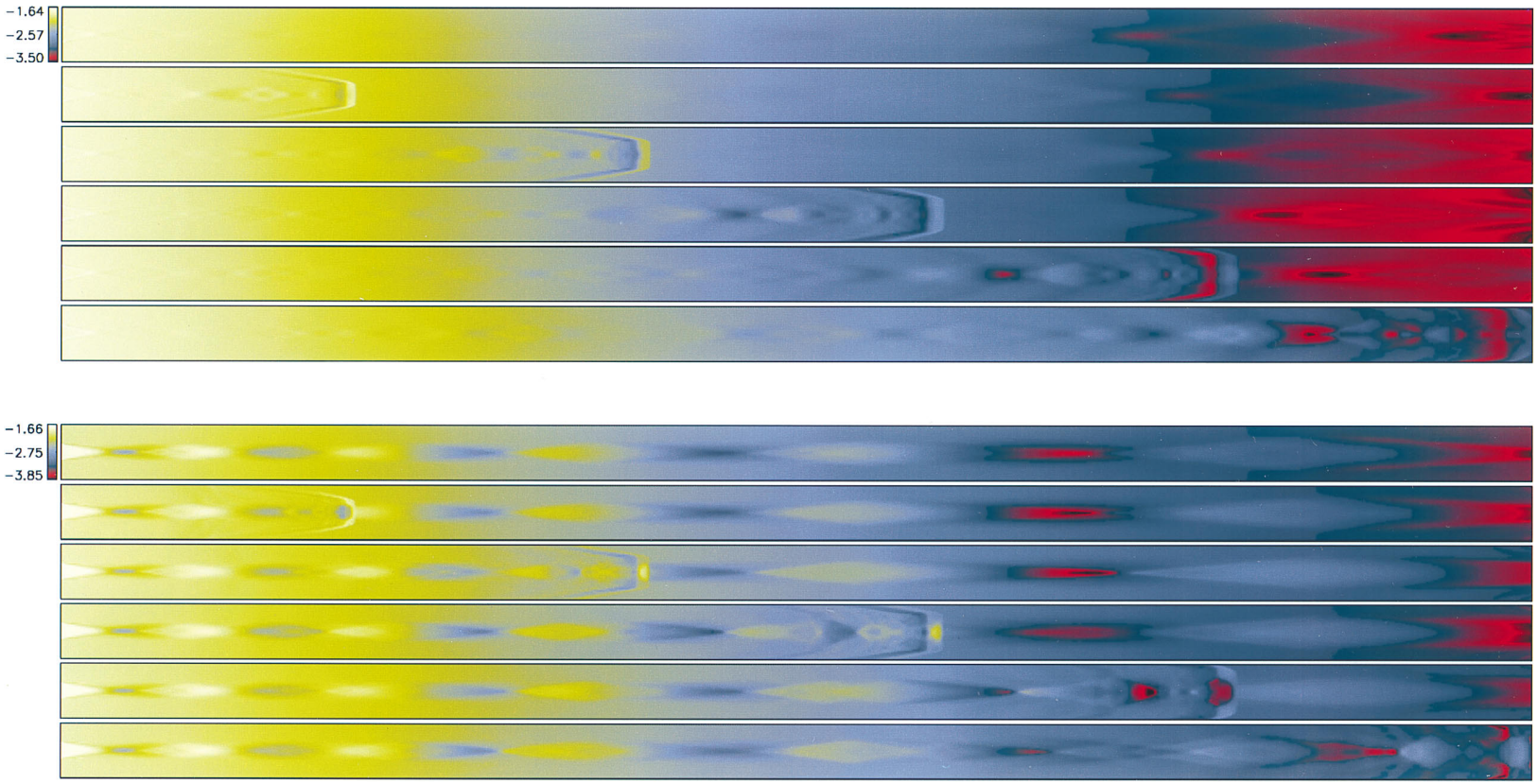

FIG. 2.—Pressure distribution at six epochs (0, 40, 80, 120, 160, and 200 R_b/c) after the introduction of a square-wave perturbation to the flow Lorentz factor for models PM (*upper panels*) and OP (*lower panels*). Owing to the decreasing pressure in the atmosphere, the jets expand with a mean opening half-angle of $\sim 0\overset{\circ}{.}4$ for both models. The simulations have been performed over a grid of 1600 × 80 cells, with a spatial resolution of 8 cells/R_b in both radial and axial directions.

GÓMEZ et al. (see 482, L34)

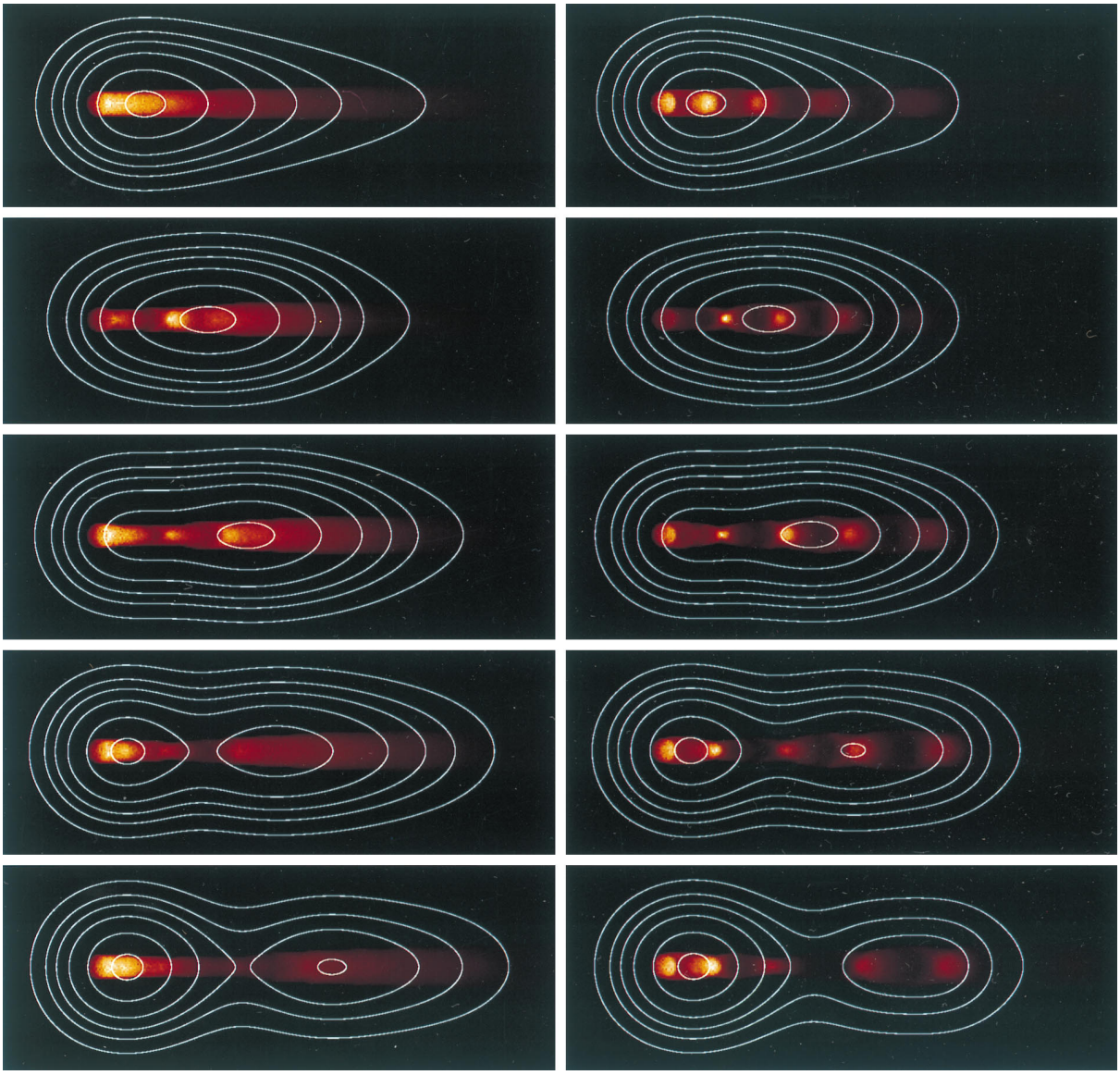

FIG. 3.—Total intensity radio maps (linear scale from dark red to bright white) of the jet models PM (*left panels*) and OP (*right panels*) at epochs 0.0, 0.9, 1.1, 1.3, and 1.5 yr in the observer's rest frame after the introduction of the perturbation. Maps correspond to optically thin 43 GHz observing frequency, and 10° viewing angle. Contours show the emission convolved with a circular Gaussian beam of FWHM 0.15 mas. Contour levels are 10%, 20%, 30%, 45%, 70%, and 95% of the peak intensity. The maps extend 0.9 mas longitudinally. To compute the emission we used the following values: spectral index of 2.2; magnetic field at the jet inlet of 20 mG; external density of 2×10^{-21} g cm^{-3}; jet radius of 0.1 pc; redshift of 0.5; Hubble constant of 80 km s^{-1} Mpc^{-1}; and ratio of maximum to minimum energy of electrons in the power-law energy distribution of 10^3.

GÓMEZ et al. (see 482, L35)